Bull. Mater. Sci., Vol. 34, No. 1, February 2011, pp. 53–60. © Indian Academy of Sciences.

# Dielectric relaxation behaviour of $Sr_2SbMnO_6$ ceramics fabricated from nanocrystalline powders prepared by molten salt synthesis

**ANTARA BARAL, K R S PREETHI MEHER and K B R VARMA***
Materials Research Centre, Indian Institute of Science, Bangalore 560 012, India

MS received 7 July 2010; revised 26 August 2010

**Abstract.** **Double perovskite polycrystalline single phase and dense $Sr_2SbMnO_6$ (SSM) ceramics, fabricated using the nanocrystalline powders synthesized by molten salt method, exhibited high dielectric constant with low dielectric loss as compared to that of SSM ceramics obtained from the powders prepared by solid-state synthesis method. The dielectric data obtained over a wide frequency (100 Hz–1 MHz) and temperature (190 K–300 K) ranges exhibited distinct relaxations owing to both the grain and grain boundary. The dielectric dispersion was modeled using the Cole–Cole equation consisting of two separate relaxation terms corresponding to the grain and grain boundary. The grain and grain boundary relaxations observed in the Nyquist plots ($Z'$ and $Z''$) were modeled by an equivalent circuit consisting of two parallel RC circuits connected in series with each other. A careful analysis of both the impedance ($Z''$ vs $\omega$) and modulus ($M''$ vs $\omega$) behaviour corroborated the conclusions drawn from the dielectric data.**

**Keywords.** **Ceramics; chemical synthesis; X-ray diffraction; dielectric properties.**

## 1. Introduction

There has been renewed interest on the materials that exhibit high ($10^4$–$10^5$) dielectric constant especially at the desired frequencies and temperatures. The incidence of high dielectric constant has been reported in different systems that include ferroelectric oxides (Yu *et al* 2005), certain transition metal oxides (Jana *et al* 2007; Thongbai *et al* 2008) and complex perovskite oxides (Keith *et al* 2004; Majhi *et al* 2007; Zhao *et al* 2007; Meher and Varma 2009). Recently, structural and magnetic characteristics of a double perovskite, $Sr_2SbMnO_6$ (SSM), which is described by a general formula, $A_2B'B''O_6$, in which $B'$ and $B''$ cations are ordered in the octahedral sites, are reported (Foster *et al* 1997; Cheah *et al* 2006; Majhi *et al* 2007; Mandal *et al* 2008; Ivanov *et al* 2009). Structural investigations into SSM prepared under different annealing conditions have been carried out by various groups. The crystal structure of SSM has been reported to be tetragonal associated with *I*4/*mcm* space group and there was a further documentation of the occurrence of Jahn Teller distortion due to the presence of $Mn^{3+}$ that contributes to the octahedral tilting (Cheah *et al* 2006; Mandal *et al* 2008; Ivanov *et al* 2009). A dielectric anomaly occurring at 450°C in SSM ceramics as a possible ferroelectric to paraelectric phase transition has been reported in the literature though the ferroelectric nature of SSM is yet to be established (Foster *et al* 1997). Further, the Colossal dielectric behaviour of SSM has been investigated in detail and it has been attributed to the Maxwell Wagner relaxation mechanism (Majhi *et al* 2007). In all the above reports, the data were on SSM that was prepared based on powders prepared by solid-state reaction route. The conventional solid-state synthesis of SSM powders from their component carbonate/oxides usually requires extensive mechanical mixing followed by prolonged heating at 135°C/48 h with a few intermediate grinding/heating cycles to achieve maximum possible homogenization. In this method, it is difficult to exercise a strict control over the microstructure, grain size etc of the resulting polycrystalline SSM powders. Therefore, there is a need to synthesize SSM by alternate low temperature routes. Further, since the temperatures involved in sintering the pellets obtained by compacting these powders are higher, there is always a possibility of cations especially Sb and Mn existing in mixed oxidation states leading to oxygen non-stoichiometry which may give rise to high dielectric loss.

This article reports the dielectric relaxation characteristics in a wide temperature and frequency range of SSM ceramics prepared using nanocrystalline powders obtained by the molten salt synthesis. The impedance and electric modulus formalisms are applied to the dielectric data which revealed the existence of electrical inhomogeneity in SSM ceramics. This approach is demonstrated to be an effective and simple method to unravel the dielectric relaxation characteristics of this type of compounds in general.

## 2. Experimental

### 2.1 *Synthesis*

Polycrystalline powders of $Sr_2SbMnO_6$ were prepared by low temperature molten-salt synthesis route. For this, a

*Author for correspondence (kbrvarma1@gmail.com)

stoichiometric mixture of AR grade $SrCO_3$, $Sb_2O_3$ and $MnO_2$ were thoroughly mixed with the eutectic composition of 0·635 $Li_2SO_4$–0·365 $Na_2SO_4$ (30 mol % salts to oxide ratio) using a planetary ball mill for 4 h in the propanol medium. The melting point of this eutectic composition is 594°C. The mixed slurry was dried at 120°C for 4 h for complete removal of propanol. The temperature of mixture of the slurry was raised to 900°C and maintained at this temperature for 10 h. Subsequently, the salts were ultrasonically washed using hot distilled water for several times to ensure that the filtrate was free from sulphate ions as confirmed by barium nitrate test. The obtained powders were fully dried at 120°C for 5 h. The full details pertaining to the synthesis of SSM nanocrystalline powders are reported elsewhere (Baral and Varma 2009).

### 2.2 *Characterization*

The phase analysis of the resultant powder was carried out by X-ray powder diffraction (XRD) using Cu K$\alpha$ radiation (Philips PW1050/37). SSM powders obtained using MSS was pressed into the pellets of 6 mm in diameter and 2 mm in thickness. The pellets were sintered at 1075°C/16 h. Rietveld refinement of XRD pattern was performed using FULLPROF program. The density of the sintered samples was around 96% of its theoretical value as confirmed by the Archimedes method using xylene as the medium. The grain size and its morphology were investigated using scanning electron microscope (SEM) (Quanta ESEM). To make electrical property measurements, gold electrodes were sputtered on both sides of the sintered pellets and copper wires were glued on to the gold coated surfaces using silver epoxy. Capacitance and dielectric loss measurements were carried out in 100 Hz–10 MHz frequency range with a signal strength of 0·5 $V_{rms}$ at various temperatures (190–300 K) using the impedance gain phase analyser (HP 4194A) in conjunction with a home-built cooling system. Based on these capacitance data, the dielectric constant, $\varepsilon'_r$, was evaluated by taking the electrode geometry of the sample into account using the formula

$$\varepsilon'_r = C.t/\varepsilon_0 A,$$

where $t$ is the thickness of the sample and $A$ the area of the electroded sample and $\varepsilon_0$ the permittivity of free space, $\varepsilon_0 = 8{\cdot}854 \times 10^{-12}$ F/m. The complex impedance ($Z^*$) and complex electric modulus ($M^*$) were evaluated using the following relations

$$Z^* = Z' - jZ'' = \frac{1}{j\omega C_0 \varepsilon^*}, \quad (1)$$

where $\omega$ is the angular frequency ($\omega = 2\pi f$) and $C_0 = \varepsilon_0 A/t$ is the empty cell capacitance where $A$ is the sample area and $t$ the sample thickness. The complex modulus could be obtained using the equation

$$M^* = M' + jM'' = \frac{1}{\varepsilon^*} = j\omega C_0 Z^*. \quad (2)$$

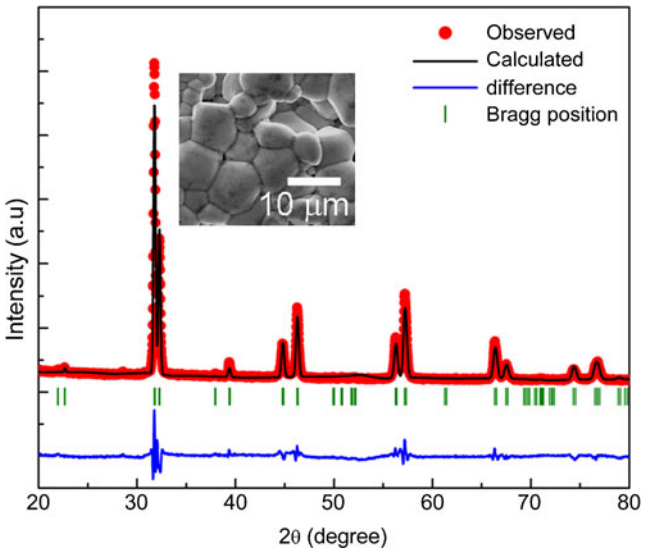


**Figure 1.** X-ray diffraction pattern of SSM Rietveld refined to space group *I*4/*mcm*. The inset shows the scanning electron micrograph of $Sr_2SbMnO_6$ ceramics sintered in air at 1075°C/16 h.

## 3. Results and discussion

### 3.1 *XRD studies*

Figure 1 represents the X-ray powder diffraction (XRD) pattern of SSM (sintered at 1075°C/16 h) recorded at room temperature. The Rietveld refinement of the XRD pattern yielded a lowest $R_{wp}$ factor of 8% for the *I*4/*mcm* (tetragonal) among other space group models such as *I*4/*m*, *I*4*mm* etc. The lattice parameters obtained from the refinement are $a = 5{\cdot}53(4)$ Å, $c = 8{\cdot}12(3)$ Å. A typical SEM micrograph of SSM pellet sintered in air at 1075°C/16 h is shown in the inset of figure 1. The microstructure reveals the well sintered nature of the pellets with grain sizes in 6–9 $\mu$m range. The faceted nature of the grains is evident by the triple junctions observed in the microstructure.

### 3.2 *Dielectric studies*

Figures 2(a) and (b) illustrate the dielectric constant ($\varepsilon'_r$) and dielectric loss ($D$) of SSM in the 190–300 K temperature range at various frequencies (100 Hz–1 MHz). At 260 K, the low frequency (100 Hz) dielectric constant is $\varepsilon'_s \sim 8{\cdot}6 \times 10^4$, whereas at the high frequency (1 MHz) dielectric constant, $\varepsilon'_\infty$ is ~180. On decreasing the temperature from 300 K, step like decrease in the dielectric constant versus temperature behaviour is observed (denoted as I and II in figure 2(a) at 1 kHz). This relaxation shifts to higher temperatures with increasing frequency. The corresponding dielectric loss peaks are marked as $P_{DI}$ and $P_{DII}$, respectively in figure 2(b) at 1 kHz. These dielectric relaxations I and II are the characteristic thermal relaxation steps very similar to that observed in the other high dielectric constant materials

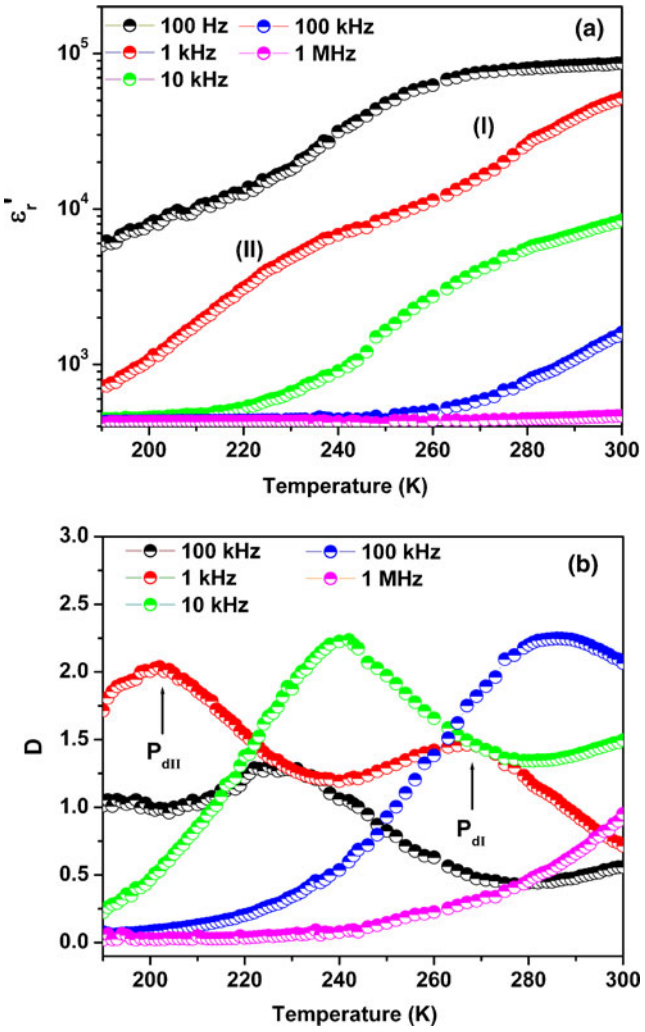


**Figure 2.** Temperature dependence of (**a**) dielectric constant ($\varepsilon_r'$) and (**b**) dielectric loss ($D$) for $Sr_2SbMnO_6$ ceramics measured at different frequencies.

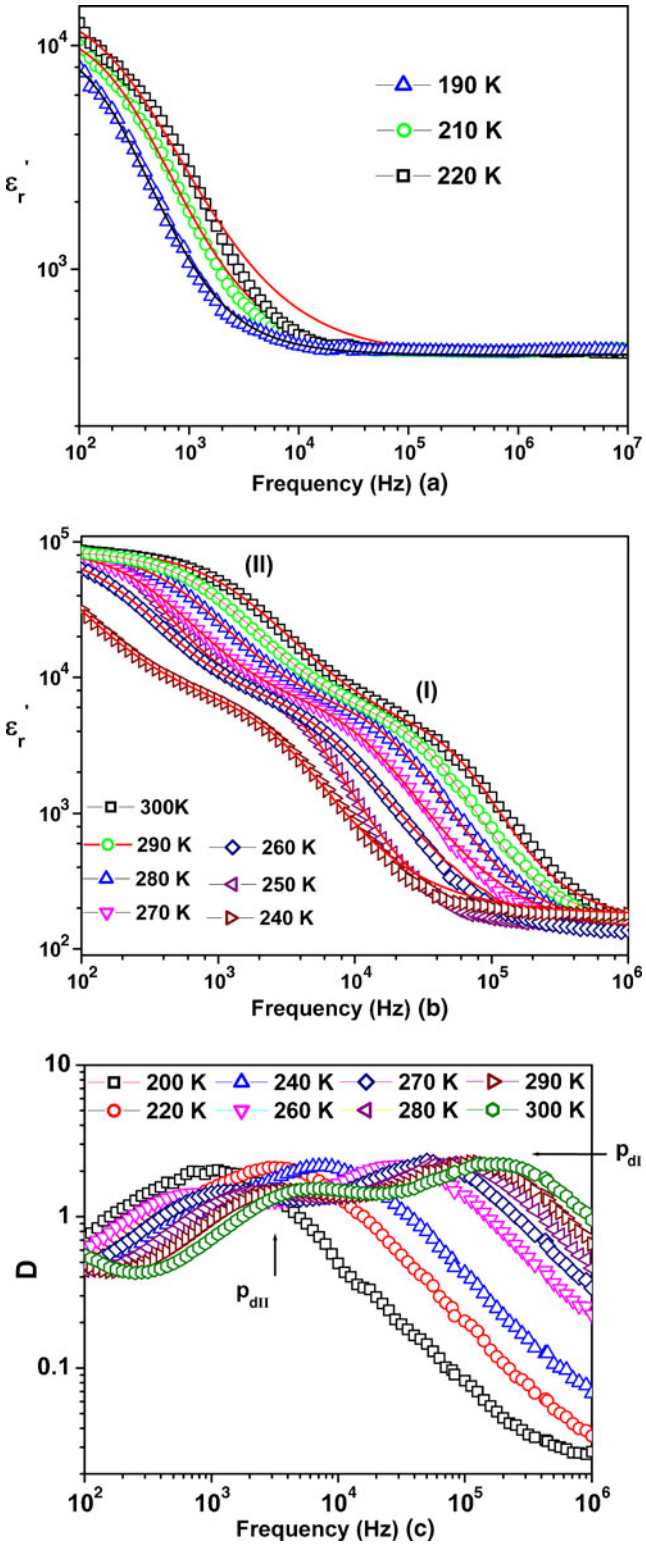


**Figure 3.** Variation of dielectric constant with frequency in (**a**) 190–220 K and (**b**) 240–300 K temperature range. Solid lines are the best theoretical fits according to (6) and (8) and (**c**) variation of dielectric loss with frequency at different temperatures.

such as $CaCu_3Ti_4O_{12}$ (CCTO) and other high dielectric constant materials (Sinclair *et al* 2002; Lunkenheimer *et al* 2004; Liu *et al* 2005; Zhang *et al* 2005; Shao *et al* 2006; Krohns *et al* 2008). Dielectric loss ($D$) exihibits a broad peak at the temperature around which the dielectric constant undergoes a thermal relaxation. At 300 K, the dielectric constant values attained are in the range of $5{\cdot}9 \times 10^4$ to 400 in the frequency range of 1–100 kHz, respectively. However, the loss values shot up due to increased conductivity at 300 K. At 190 K, the dielectric constant falls in the range of ~700–100 for the same frequency range with $D$ values being less as the conductivity is lower at this temperature.

The dielectric relaxations I and II can be more systematically analysed from the frequency response of the dielectric constant ($\varepsilon_r'$) and dielectric loss ($D$). Figures 3(a)–(c) show the variation of $\varepsilon_r'$ and $D$ with frequency at various temperatures in the temperature range 190–300 K. The dielectric dispersion at various temperatures (190–300 K) has been analysed using Cole–Cole formalism. At 190–220 K, dielectric constant exhibits a single relaxation step (I)

with the corresponding loss peak ($P_{\mathrm{DI}}$) observed in the loss spectra (figures 3(a) and 3(c)). However, with the increase in temperature above 240 K, there are two relaxations (which are marked as I and II) in figure 3(b) accompanied by the corresponding dielectric loss peaks (denoted as $P_{\mathrm{DI}}$ peak and $P_{\mathrm{DII}}$ peak, respectively as shown in figure 3(c)).

To begin with, an attempt has been made to rationalize the nature of dielectric relaxation in SSM by using the Cole–Cole equation (Cole and Cole 1941). The experimental dielectric permittivity curves for 190 K $\leq T \leq$ 220 K in figure 3(a) can be described by

$$\varepsilon'_{\mathrm{r}} = \mathrm{Re}\left\{\varepsilon'_{\infty} + \left(\varepsilon'_0 - \varepsilon'_{\infty}\right)/\left[1 + (i\omega\tau)^{\beta}\right]\right\}, \tag{3}$$

where $\varepsilon'_0$ is the static dielectric constant, $\varepsilon'_{\infty}$ the dielectric constant at higher frequency and $\omega = 2\pi f$ is the angular frequency, $(\varepsilon'_0 - \varepsilon'_{\infty})$ the dielectric relaxation strength, $\tau$ is the relaxation time and $\beta$ a constant, which varies from 0 to 1 ($\beta = 1$ for an ideal Debye relaxation involving a single characteristic relaxation time). From (3), $\varepsilon'_{\mathrm{r}}$ can be rewritten as

$$\varepsilon'_{\mathrm{r}} = \varepsilon'_{\infty} + \left(\varepsilon'/2\right) \times \{1 - \sinh(\beta z)/[\cosh(\beta z) + \cos(\beta\pi/2)]\}, \tag{4}$$

where $z = \ln(\omega\tau)$. To fit the experimental curves for 240 K $\leq T \leq$ 300 K, the entire frequency range can be modelled by including an extra relaxation term in (3) in order to account for the additional relaxation, which is given by

$$\varepsilon'_{\mathrm{r}} = \varepsilon'_{\infty} + \left(\varepsilon'/2\right)\left\{1 - \frac{\sinh(\beta_1 z_1)}{[\cosh(\beta_1 z_1) + \cos(\beta_1\pi/2)]}\right\} + \left(\varepsilon'/2\right)\left\{1 - \frac{\sinh(\beta_2 z_2)}{[\cosh(\beta_2 z_2) + \cos(\beta_2\pi/2)]}\right\}, \tag{5}$$

where $z_1 = \ln(\omega\tau_1)$ and $z_2 = \ln(\omega\tau_2)$. $\varepsilon'_1$, $\varepsilon'_2$, $\tau_1$, $\tau_2$ are the dielectric relaxation strengths and relaxation times associated with dielectric relaxations I and II (marked in figure 3(b)). $\beta_1$ and $\beta_2$ are the corresponding dispersion constants whose values can vary from 0 to 1. The $\varepsilon'_{\infty}$ value considered in each case is ~110 which is the dielectric constant obtained at a frequency of 1 MHz at 190 K. By fitting the experimental data that were obtained above 252 K to (5), the parameters $\varepsilon'_1$, $\varepsilon'_2$, $\beta_1$, $\beta_2$. $\tau_1$, $\tau_2$ could be obtained as functions of temperature. The solid lines in figures 3(a) and (b) are the mathematical fit of the experimental results according to (4) (for $T < 240$ K) and (5) (for $T > 240$ K), respectively. The values obtained for $\tau_1$ and $\tau_2$ at 260 K are $11{\cdot}14 \times 10^{-7}$ s and $19{\cdot}54 \times 10^{-5}$ s, respectively.

As the relaxation process is thermally activated, the relaxation time follows the Arrhenius law, $\tau = \tau_0 \exp(E_{\mathrm{a}}/K_{\mathrm{B}}T)$, where $\tau_0$ is the pre-exponential factor (or the relaxation time at infinite temperature), $E_{\mathrm{a}}$ denotes the activation energy of the relaxation process, $T$ the absolute temperature, and $K_{\mathrm{B}}$ the Boltzmann constant. The relaxation parameters, $E$ and $\tau_0$, can be deduced from the slope and the intercept of the Arrhenius plots. Figures 4(a) and (b) show the Arrhenius plots corresponding to two dielectric relaxations observed in the dielectric data. The relaxation parameters, $E_{\mathrm{II}} = 0{\cdot}35$ (2) eV, $\tau_{0\mathrm{II}} = 3{\cdot}2 \times 10^{-10}$ s, for the $P_{\mathrm{DII}}$ peak (figure 4(a)), and $E_{\mathrm{I}} = 0{\cdot}26$ (2) eV, $\tau_{0\mathrm{I}} = 4{\cdot}01 \times 10^{-11}$ s for the $P_{\mathrm{DI}}$ peak (figure 4(b)) are obtained. The activation energy of 0·26 eV has been reported to be equivalent to the activation energy required for the thermal motion of $Mn^{3+}$ cations within the oxygen octahedra (Iguchi and Lee 1993).

High dielectric constant associated with SSM ceramics has its origin in the extrinsic mechanism such as interfacial polarization arising at the grain/grain boundary interface. The dielectric behaviour of SSM ceramics prepared by solid-state reaction route exhibits a dielectric loss as high as ~10 around its characteristic relaxation frequency at room temperature (Majhi *et al* 2007). This has been attributed to the hopping electronic conduction among the multiple valencies of Mn cation which occurs due to the loss of oxygen at very high sintering temperatures. By considerably reducing the sintering temperature by MSS method, the maximum dielectric loss has been significantly brought down without compromising its high dielectric constant behaviour. Table 1

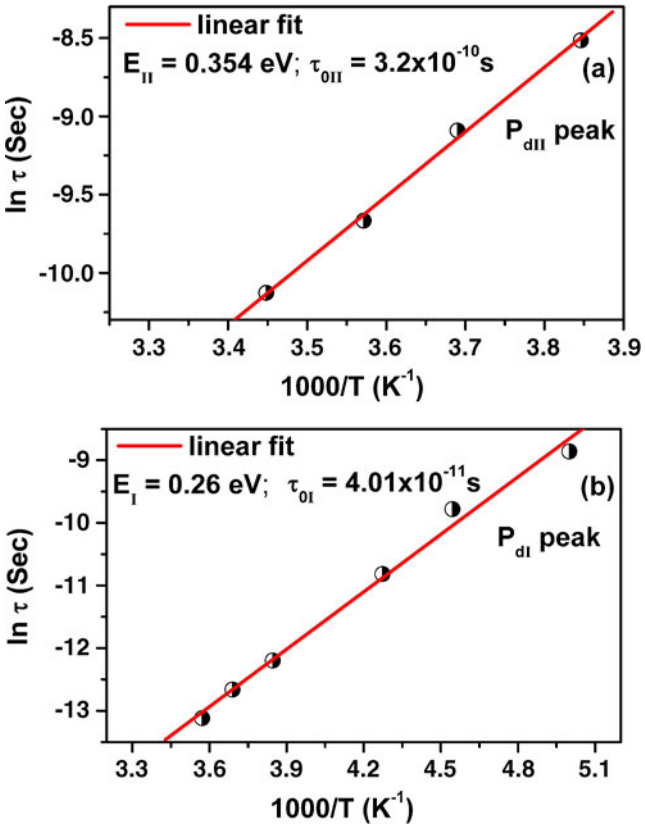


**Figure 4.** Relaxation time as a function of $1/T$ for the two dielectric relaxation peaks (**a**) $P_{\mathrm{dII}}$ and (**b**) $P_{\mathrm{dI}}$ observed in the dielectric loss spectra. The solid lines represent the linear fit.

**Table 1.** Illustrates the dielectric data at selected frequencies at 300 K obtained for the present ceramics along with that of ceramics fabricated from the powders prepared by solid state reaction route.

| | SSM (solid-state reaction route) | | SSM (molten salt synthesized) | |
|---|---|---|---|---|
| Frequency (kHz) | $\varepsilon'_r$ | $D$ | $\varepsilon'_r$ | $D$ |
| 0·1 | $\sim 1{\cdot}3 \times 10^5$ | 30 | 84,500 | 0·55 |
| 1 | $\sim 1{\cdot}2 \times 10^5$ | 3·73 | 51,000 | 0·715 |
| 10 | 74,000 | 2·5 | 7900 | 1·49 |

illustrates the dielectric data at selected frequencies obtained for the present ceramics along with that of ceramics fabricated from the powders prepared by solid state reaction route. Further, one can look at the dielectric dispersion data in terms of impedance and electric modulus simultaneously in order to ascertain the cause for such a distinct dielectric behaviour.

### 3.3 *Impedance spectroscopy*

The complex impedance $Z^*$ can be calculated from $\varepsilon^*$ according to (1). Figure 5 shows the frequency dependence of the imaginary part of impedance in the temperature range 190–300 K. At 190 K, a peak is observed in $Z''(\omega)$ (denoted as $P_{ZI}$) that shifts to high frequency range with increasing temperature. Above 250 K, another relaxation peak (denoted as $P_{ZII}$) emerges at the lower frequency side of $Z''(\omega)$, which shifts to higher frequency with further increase in temperature. The two peaks $P_{ZI}$ and $P_{ZII}$ actually corresponds to the two relaxation peaks $P_{DI}$ and $P_{DII}$ that were observed in the dielectric loss spectra within the measured frequency range.

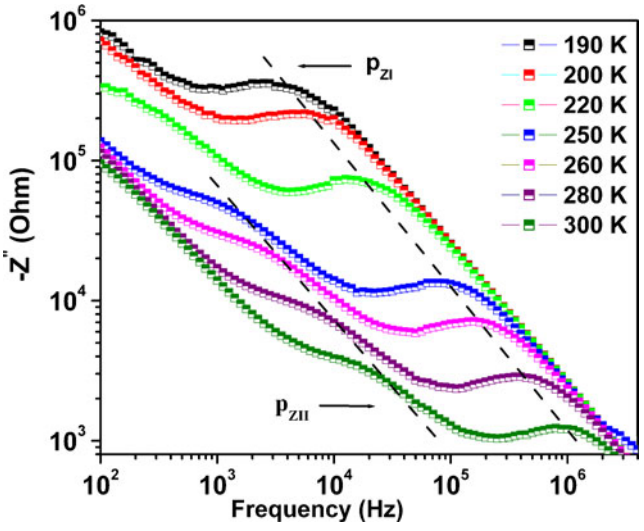


**Figure 5.** Frequency dependence of the imaginary part of $Z^*$ obtained at various temperatures. The solid lines are the guidance to eyes indicating the shift in the relaxation peaks with increasing temperature.

Cole–Cole representation is more convenient to distinguish between the bulk and grain boundary effects exhibited by certain paraelectric/ferroelectric compounds (Irvine *et al* 1990; Donald 2005). The complex impedance plane plot ($Z''$ vs $Z'$), also called Nyquist plot, where real $Z'$ represents the resistive part and the $Z''$ values represent the capacitive part, is generally used. When more than one dielectric relaxation is involved, this complex representation of the dielectric data is used to evaluate the resistance ($R$) and capacitance ($C$) values associated with each of them.

Figures 6(a) and (b) present the impedance spectra of the SSM ceramic measured at various temperatures. Above 240 K, the two well resolved semicircular arcs and a short spike are attributed to the grain, grain boundary, and the interface between the sample and electrode, respectively. This behaviour could be best modelled using Maxwell Wagner type of relaxation by invoking an equivalent circuit consisting of a series of two constant phase elements (CPEs) (non-ideal capacitor behaviour) connected in parallel to the corresponding resistors as shown in the inset of figure 6(c). This type of behaviour could be explained by the Cole–Cole complex impedance equation (Sinclair *et al* 2002) viz.

$$Z' - jZ'' = \frac{R_1}{1 + A_1 (j\omega)^{\beta} R_1} + \frac{R_2}{1 + A_2 (j\omega)^{\beta} R_2}, \quad (6)$$

where $A_1$ and $A_2$ are constants that are independent of frequency, $\omega$ is the angular frequency and $\beta$ $(0 < \beta \leq 1)$ represents the departure from the ideal Debye response. The impedance associated with CPE could be described as $Z^*_{CPE} = 1/[A (j\omega)^{\beta}]$. The CPE can be treated as an ideal capacitor ($C = A$) for $\beta = 1$. The observed $Z^*$ behaviour is modelled to (6) using the impedance analysis software Z-VIEW (demo version, 1990). A series resistor ($R_s$) is added to the circuit to account for the nonzero intercept on the real axis of the impedance plot. The fit parameters obtained for the impedance data at 250 K (figure 6(c)) such as ($R_g$, $R_{gb}$), ($A_g$, $A_{gb}$) and ($\beta_g$, $\beta_{gb}$) representing the resistive and capacitive elements associated with the high and low frequency grain and grain boundary dielectric response, are listed in table 2. The $A_g$ value is characteristic of other bulk ferroelectrics and the $A_{gb}$ value reveals that the sample is well sintered, with narrow intergranular regions (Iguchi and Lee 1993). The calculated $A_g$ and $A_{gb}$ values are also consistent

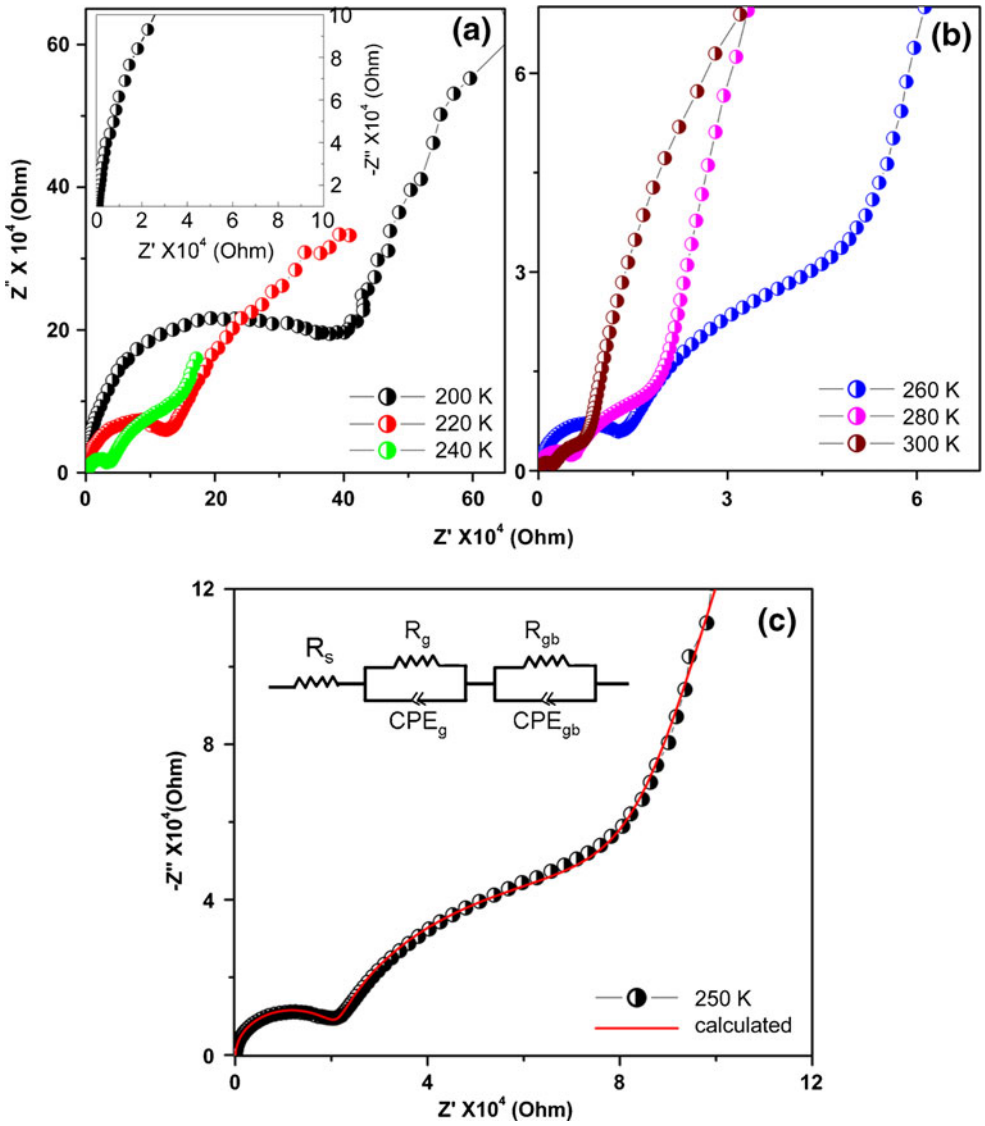


**Figure 6.** Impedance complex plot, $Z^*$ ($-Z''$ vs $Z'$) (**a**) 200–240 K, the inset in the figure shows a magnified view of the high frequency data, (**b**) 260–300 K and (**c**) at 250 K where the solid line indicates the best mathematical fit. Inset is the equivalent circuit used to model the impedance spectra.

with the measured values in dielectric spectroscopy. Therefore, we attribute the two relaxation processes to the bulk and the grain boundary effects.

The electrical conductivity (σ) of the sintered samples could be calculated from the $R$ values associated with grain and grain boundary relaxations observed in the impedance spectra. Table 3 lists the grain and grain boundary conductivity values obtained at 200 K and 300 K, where the grain conductivity is higher than that of the grain boundary indicating an electrical heterogeneity associated with the sample.

**Table 2.** Estimated fit parameters of the equivalent circuit at 250 K for SSM.

| Fit parameters | Values | Fit parameters | Values |
|---|---|---|---|
| $R_s$ | 62·95 (Ω) | $R_{gb}$ | $1{\cdot}9 \times 10^5$ (Ω) |
| $R_g$ | $2{\cdot}5 \times 10^4$ (Ω) | $A_{gb}$ | $1{\cdot}6 \times 10^{-9}$ (Ω) |
| $A_g$ | $7 \times 10^{-11}$ (F) | $\beta_{gb}$ | 0·84 |
| $\beta_g$ | 0·98 | | |

**Table 3.** Typical conductivity values of grain and grain boundary observed at 200 K and 300 K.

| Temperature (K) | Grain (S/m) | Grain boundary (S/m) |
|---|---|---|
| 200 | $0{\cdot}91 \times 10^{-4}$ | $0{\cdot}02 \times 10^{-5}$ |
| 300 | $0{\cdot}19 \times 10^{-2}$ | $0{\cdot}85 \times 10^{-5}$ |

Figure 7 shows separate Arrhenius plots (log $\sigma$ vs 1000/$T$) for these two relaxations. The activation energy calculated from the Arrhenius plots are 0·28 (2) eV and 0·33 (2) eV for the grain and the grain boundary, respectively. This is in close agreement with the activation energies calculated from the dielectric loss spectra.

### 3.4 *Electric modulus studies*

The electric modulus ($M^*$) is another physical representation of the dielectric relaxation process. The real ($M'$) and imaginary ($M''$) parts of $M^*$ in terms of the resistances and capacitances associated with grain and grain boundary are expressed as

$$M' = \frac{C_0}{C_g}\left[\frac{(\omega R_g C_g)^2}{1+(\omega R_g C_g)^2}\right] + \frac{C_0}{C_{gb}}\left[\frac{(\omega R_{gb} C_{gb})^2}{1+(\omega R_{gb} C_{gb})^2}\right], \tag{7}$$

and

$$M'' = \frac{C_0}{C_g}\left[\frac{\omega R_g C_g}{1+(\omega R_g C_g)^2}\right] + \frac{C_0}{C_{gb}}\left[\frac{\omega R_{gb} C_{gb}}{1+(\omega R_{gb} C_{gb})^2}\right]. \tag{8}$$

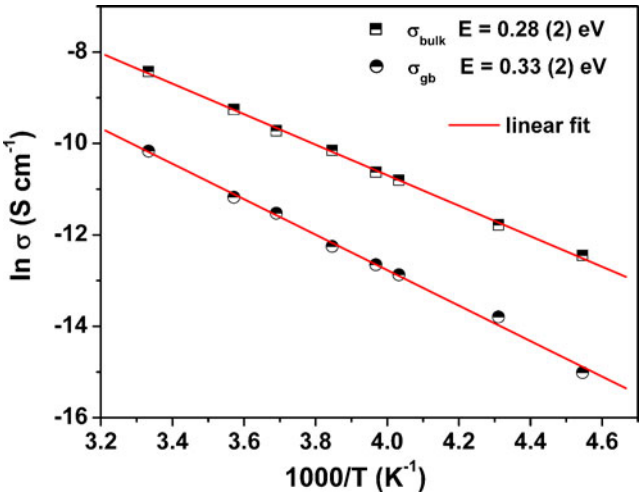


**Figure 7.** Grain and grain boundary conductivity as a function of the inverse of temperature. Solid lines are the linear fit to the experimental data.

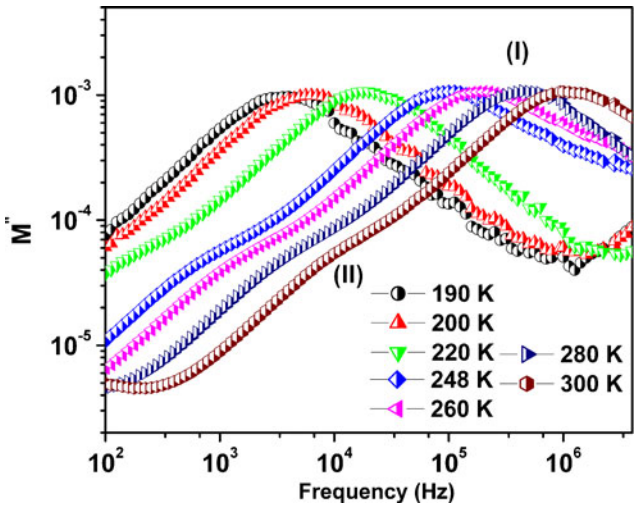


**Figure 8.** Frequency dependence of the imaginary part of the dielectric modulus measured at various temperatures.

Figure 8 shows the frequency dependence of $M''$ at various temperatures. According to (7) and (8), the relaxation peaks occur at frequencies $1/(2\pi R_g C_g)$ and $1/(2\pi R_{gb} C_{gb})$, respectively. Since peak values are proportional to the reciprocal of the associated capacitances, the relaxation associated with smaller capacitance gives maximum intensity peak in the electric modulus plots. Therefore, peak associated with the grains is of higher intensity than that of the grain boundaries. The broadening of $M''$ peaks compared to an ideal Debye peak indicates heterogeneity associated with the microstructure of the material which leads to a spatial distribution of local conductivity and electrical response times (Gerhardt 1994). At low temperatures, a single relaxation peak observed in $M''$ vs frequency corresponds to the grain response (marked as I in figure 8). With increasing temperature, the peaks corresponding to the grain relaxation shifts towards higher frequencies and another closely occurring shoulder (marked as II in figure 8) corresponding to grain boundary response occurs at the low frequency side. The modulus plots in general do not give any signature of the capacitance arising due to the interfacial electrode polarization.

## 4. Conclusions

In conclusion, $Sr_2SbMnO_6$ ceramics prepared by MSS method exhibited better dielectric behaviour with high dielectric constant and a significant decrease in the dielectric loss. The temperature and frequency dependence of the dielectric spectra, impedance and electric modulus have been investigated in detail. An excellent fit between the experimental and calculated dielectric relaxation was obtained over a wide frequency and temperature domain using the modified Cole–Cole equation. The overall dielectric behaviour is attributed to the grain and grain boundary effects distinguished based on the values of capacitance, resistance and relaxation times. The colossal dielectric behaviour has its origin in the Maxwell Wagner type relaxation mechanism that arises due to the conducting grain separated by resistive grain boundaries ($R_{gb} \gg R_g$ and $C_{gb} \approx 10 C_g$).

**Acknowledgement**

The authors thank Joint Advanced Technology program (JATP) of Defence Research and Development Organization (DRDO), Government of India, for financial assistance.

**References**

Baral A and Varma K B R 2009 *J. Solid State Chem.* **182** 3282
Cheah M, Saines P J and Kennedy B J 2006 *J. Solid State Chem.* **179** 1775
Cole K S and Cole R S 1941 *I. J. Chem. Phys.* **9** 341
Donald J R M 2005 *Impedance spectroscopy* (New York: John Wiley)
Foster M C, Nielson R M and Abraham S C 1997 *J. Appl. Phys.* **82** 3076
Gerhardt R 1994 *J. Phys. Chem. Solids* **55** 1491
Iguchi E and Lee K J 1993 *J. Mater. Sci.* **28** 5809
Irvine J T S, Sinclair D C and West A R 1990 *Adv. Mater.* **2** 132
Ivanov S A, Nordblad P, Tellgren R and Hewat A 2009 *Mater. Res. Bull.* **44** 822
Jana P K, Sarkar S and Chaudhuri B K 2007 *J. Appl. Phys.* **90** 242913
Keith G M, Kirk C A, Sarma K, McNAlford N, Cussen E J, Rosseinsky M J and Sinclair D C 2004 *Chem. Mater.* **16** 2007
Krohns S, Lunkenheimer P, Ebbinghaus S G and Loidl A 2008 *J. Appl. Phys.* **103** 084107
Liu J, Duan C-g, Mei W N, Smith R W and Hardy J R 2005 *J. Appl. Phys.* **98** 093703
Lunkenheimer P, Fichtl R, Ebbinghaus S G and Loidl A 2004 *Phys. Rev.* **B70** 172102
Majhi K, Prakash B S and Varma K B R 2007 *J. Phys. D: Appl. Phys.* **40** 7128
Mandal T K, Poltavets V V, Croft M and Greenblatt M 2008 *J. Solid State Chem.* **181** 2325
Meher K R S P and Varma K B R 2009 *J. Appl. Phys.* **105** 034113
Shao S F, Zhang J L, Zheng P, Zhong W L and Wang C L 2006 *J. Appl. Phys.* **99** 084106
Sinclair D C, Adams T B, Morrison F D and West A R 2002 *Appl. Phys. Lett.* **80** 2153
Thongbai P, Yamwong T and Maensiri S 2008 *Solid State Commun.* **147** 385
Yu J, Ishikawa T, Arai Y, Yoda S, Itoh M and Saita Y 2005 *Appl. Phys. Lett.* **87** 252904
Zhang J L, Zheng P, Wang C L, Zhao M L, Li J C and Wang J F 2005 *Appl. Phys. Lett.* **8** 742901
Zhao F, Yue Z, Pei J, Yang D, Gui Z and Li L 2007 *Appl. Phys. Lett.* **91** 052903